ACS APPLIED MATERIALS & INTERFACES

Research Article

www.acsami.org

# Dually Actuated Triple Shape Memory Polymers of Cross-Linked Polycyclooctene–Carbon Nanotube/Polyethylene Nanocomposites

Zhenwen Wang,[†] Jun Zhao,*[,†,∥] Min Chen,[†] Minhao Yang,[†] Luyang Tang,[†] Zhi-Min Dang,*[,†] Fenghua Chen,[‡] Miaoming Huang,[§] and Xia Dong*[,§]

[†]Department of Polymer Science and Engineering, School of Chemistry and Biological Engineering, University of Science and Technology Beijing, Beijing 100083, People's Republic of China

[‡]Laboratory of Advanced Polymer Materials, Beijing National Laboratory for Molecular Sciences, Institute of Chemistry, Chinese Academy of Sciences, Beijing 100190, People's Republic of China

[§]CAS Key Laboratory of Engineering Plastics, Beijing National Laboratory for Molecular Sciences, Institute of Chemistry, Chinese Academy of Sciences, Beijing 100190, People's Republic of China

*S* *Supporting Information*

**ABSTRACT:** In this work, electrically and thermally actuated triple shape memory polymers (SMPs) of chemically cross-linked polycyclooctene (PCO)–multiwalled carbon nanotube (MWCNT)/polyethylene (PE) nanocomposites with co-continuous structure and selective distribution of fillers in PCO phase are prepared. We systematically studied not only the microstructure including morphology and fillers' selective distribution in one phase of the PCO/PE blends, but also the macroscopic properties including thermal, mechanical, and electrical properties. The co-continuous window of the immiscible PCO/PE blends is found to be the volume fraction of PCO ($\nu^{PCO}$) of ca. 40–70 vol %. The selective distribution of fillers in one phase of co-continuous blends is obtained by a masterbatch technique. The prepared triple SMP materials show pronounced triple shape memory effects (SMEs) on the dynamic mechanical thermal analysis (DMTA) and the visual observation by both thermal and electric actuations. Such polyolefin samples with well-defined microstructure, electrical actuation, and triple SMEs might have potential applications as, for example, multiple autochoke elements for engines, self-adjusting orthodontic wires, and ophthalmic devices.

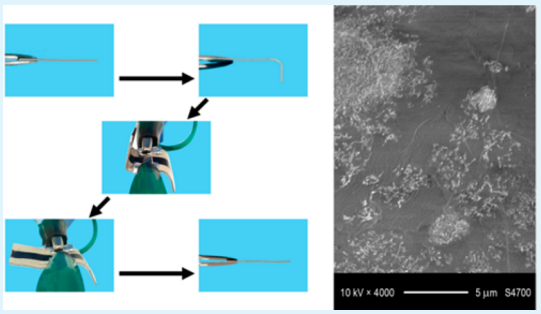


**KEYWORDS:** *electrical actuation, triple shape memory effects, polyolefins, nanocomposites, co-continuous structure, selective distribution*

## INTRODUCTION

Shape memory polymers (SMPs) can remember their permanent macroscopic shape, be frozen to a temporary shape under some specific conditions, and then recover to their original shape under external stimuli.[1−3] Compared with the widely used shape-memory alloys and ceramics (SMAs and SMCs, respectively), SMPs have some great advantages such as large strain, low density, easy processing, broad operation temperature, tunable elastic modulus and switch temperature ($T_{sw}$), and potential biocompatibility and biodegradability.[4−19]

However, SMPs also have some disadvantages such as relatively low elastic modulus and lack of functions.[20] To solve these problems, introducing functional inorganic or metallic fillers into the polymer matrix to prepare SMP composites has become a popular strategy.[21−23] In this way, both mechanical and thermal properties of the materials could be significantly improved.[24−27] Moreover, instead of direct heating, some new actuations such as electrical, magnetic, optical, and chemical stimuli could be achieved.[28−37] Among them, electrical stimulation by adding conductive fillers such as carbon materials and metals has attracted the most attention because of potential industrial applications.[38−42] For example, temporally and spatially controlled shape memory effect (SME) was obtained for electrically conductive polymer nanocomposites with carbon nanotube (CNT) as fillers.[43]

The double SMPs generally have a permanent shape and only a single temporary shape. In contrast, triple and multiple SMPs could provide more complex actuation because they have two or more temporary shapes besides their permanent shape.[44−48] Generally, double SMPs need only a reversible phase, while triple and multiple SMPs need two or more reversible phases, respectively. An interesting strategy to get triple and even multiple SMEs was to use the broad glass transition of polymers.[6,49,50] Besides, triple SMEs were also realized in a system comprised of a permanent covalent cross-linking and a supramolecular hydrogen bonding cross-linking.[51]

**Received:** August 20, 2014
**Accepted:** October 27, 2014
**Published:** October 27, 2014

  

In our previous work, triple SMPs were prepared by chemically cross-linking immiscible blends of two kinds of polyolefins, polyethylene (PE)/polypropylene (PP) with well-defined co-continuous structure.[52] The co-continuous structure was built up in the samples to get some synergetic enhancement of the mechanical properties. Polyolefins PE and PP were used because of their mass production and substantial cost advantage as general plastics. The new strategy proved to be useful in the design of novel triple SMPs. This work provides a further development of the novel strategy. While PE with the melting temperature ($T_m$) of ca. 110 °C was kept as a component of the blends, another component, polycyclooctene (PCO) with low $T_m$ of ca. 55 °C, was used to replace PP, which has a high $T_m$ of 165 °C.[53−56] Such PCO/PE blends could be used to prepare triple SMPs with lower $T_{sw}$ values. Electrically conductive multiwalled carbon nanotubes (MWCNTs) were selectively distributed in the PCO phase by using a masterbatch technique for the electrical actuation.[57−60] Such efforts of combining electrical actuation and triple SMPs with well-defined microstructure should be helpful to the academic understanding and industrial applications of new SMP materials.

## RESULTS AND DISCUSSION

**Co-continuous Structure Built up in PCO/PE Blends and Selective Distribution of MWCNT Fillers in PCO Phase of the Blends.** The microstructure of two-component blends depends on the volume fraction of each component and the compatibility between them. Figure 1 shows the scanning electronic microscopy (SEM) images of the cryo-fractured surface of the PCO/PE blends with various volume fractions of PCO component ($v^{PCO}$). The same strategy as in our previous work is used to extract one component of the blends by using two components' different solubility at the same temperature.[52] That is, although xylene is an excellent solvent for both PCO and PE at a high enough temperature (e.g., 90.0 °C, and a long time of dissolution is needed), PCO is more soluble than PE at a lower temperature (e.g., 60.0 °C) because of the much lower $T_m$ of PCO (ca. 55 °C) than that of PE (ca. 110 °C). Therefore, PCO could be selectively extracted after a short time of 15 min at 60.0 °C, while most of the PE remains undissolved in this condition. From Figure 1, it can also be seen that for the blends with $v^{PCO}$ of 10 vol %, the PCO component is the dispersed phase with a diameter of less than 1 μm, while the PE component is the continuous matrix, which is a so-called sea−island structure. For the blends with $v^{PCO}$ of 30 vol %, the PE component is still the continuous matrix. Some PCO might already form some kind of continuous phase in the system based on the solvent extraction measurements, but most of it is still a dispersed phase with a diameter of 1−3 μm in the PE matrix. For the blends with $v^{PCO}$ of 50 vol %, both PCO and PE components form the continuous matrix and a well-defined co-continuous structure with a domain diameter of ca. 3−7 μm is built up in the system. For the blends with $v^{PCO}$ of 70 vol %, PCO is the continuous matrix with a domain diameter of ca. 5−10 μm, while PE also forms a continuous phase with a domain diameter of ca. 1−3 μm. Therefore, a co-continuous structure is also formed in the system. For the blends with $v^{PCO}$ of 90 vol %, PCO component is the continuous matrix, while PE component forms the dispersed phase with a diameter of less than 1 μm (SEM micrographs are not given). On the basis of these results, it is clear that the co-continuous window of PCO/PE blends is the $v^{PCO}$ of ca. 40−70 vol %, which is in contrast to the co-continuous window of the volume fraction of ca. 30−70 vol % for the PE/PP blends.[52] It is reasonable to assume that the co-continuous structure will be kept after chemical cross-linking of the blends to prepare SMPs. Cross-linking both phases of the co-continuous structure could provide double networks in the system for the production of triple SMPs with high fixity ratio and recovery ratio.[52]

Figure 2 presents the SEM images of the cryo-fractured surface of liner and cross-linked PCO-MWCNT 8 vol % and PCO-MWCNT 15 vol %/PE 70/30 vol % nanocomposites. According to Figure 2a, MWCNT fillers are homogeneously dispersed in the PCO matrix. Electrically conductive networks are well formed in the system. As shown in Figure 2b, MWCNT fillers are selectively distributed in the PCO phase of the PCO/PE blends. Therefore, two distinct regions can be seen: a PCO phase containing MWCNT fillers and a PE phase almost free of fillers. Both PCO and PE components form the continuous matrix of the system with a channel width of ca. 1−5 μm. Figure 2c,d shows that the chemical cross-linking has some significant influence on the morphology of the samples. Compared with linear blends shown in Figure 2a,b, the boundary between different phases of cross-linked blends

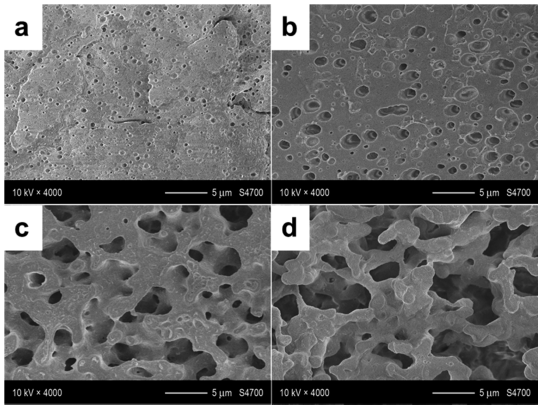


**Figure 1.** SEM images of the cryo-fractured surface of PCO/PE blends with various $v^{PCO}$: (a) 10 vol %, (b) 30 vol %, (c) 50 vol %, and (d) 70 vol %. PCO has been dissolved with xylene.

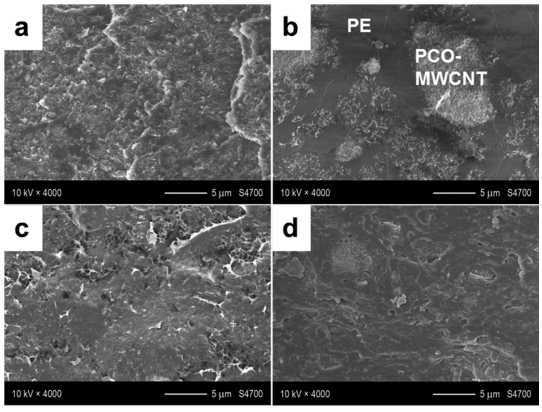


**Figure 2.** SEM images of the cryo-fractured surface of (a) linear PCO-MWCNT 8 vol %, (b) linear PCO-MWCNT 15 vol %/PE 70/30 vol %, (c) cross-linked PCO-MWCNT 8 vol %, and (d) cross-linked PCO-MWCNT 15 vol %/PE 70/30 vol % nanocompsoites. PCO-MWCNT and PE phases are marked in panel b.

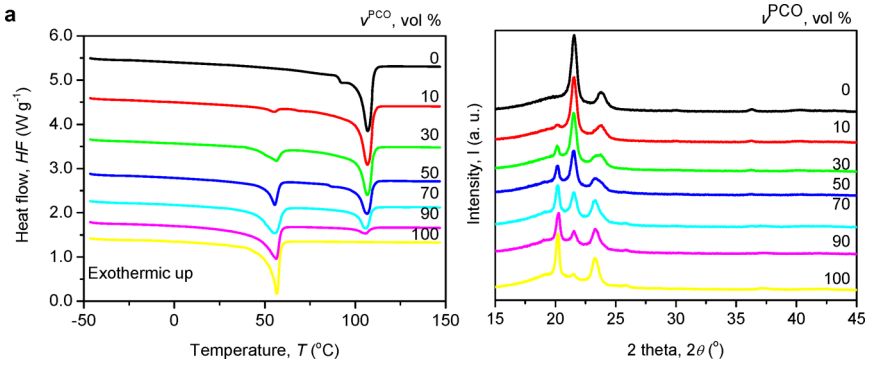


**Figure 3.** (a) DSC thermographs of HF during heating and (b) WAXD patterns of PCO/PE blends with various $v^{PCO}$.

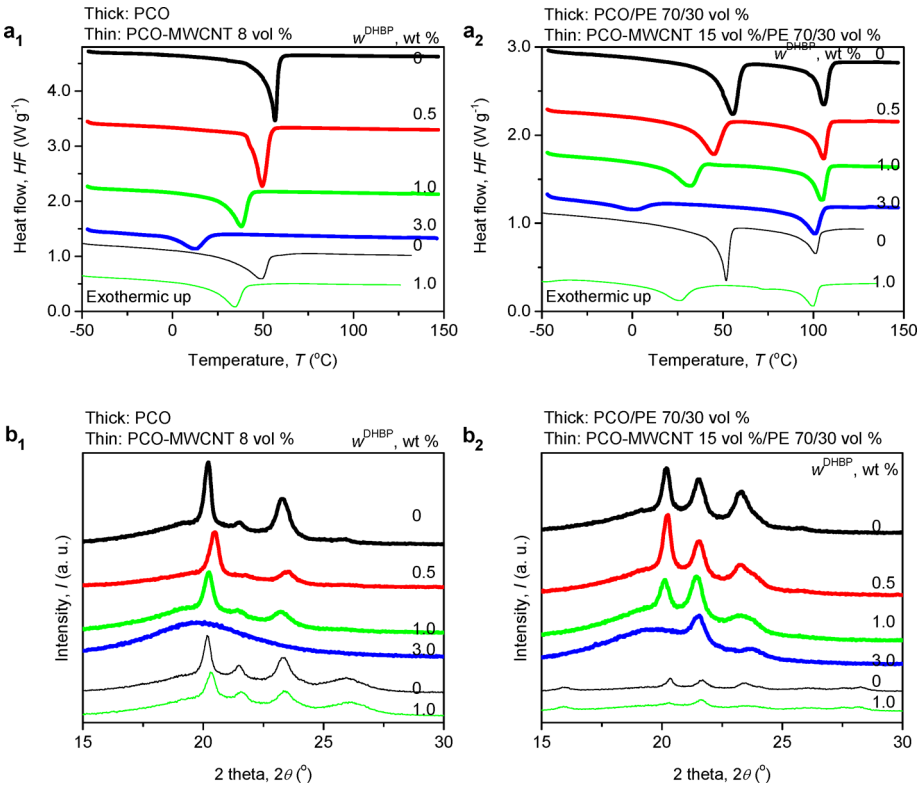


**Figure 4.** (a) DSC thermographs of HF during heating and (b) WAXD patterns of ($a_1$ and $b_1$) PCO and PCO-MWCNT 8 vol % nanocomposites and ($a_2$ and $b_2$) PCO/PE 70/30 vol % blends and PCO-MWCNT 15 vol %/PE 70/30 vol % nanocomposites cross-linked by various $w^{DHBP}$.

becomes less visible. Besides, some kind of agglomeration of fillers might happen during the chemical cross-linking because the initiator, 2,5-dimethyl-2,5-di(*tert*-butylperoxy)-hexane (DHBP) could also react with the fillers' surface and change its characteristics. Actually, the electrically conductive networks in the system are also affected by the chemical reaction, as will be shown below for the electrical conductivity ($\sigma_e$).

**Thermal Properties and Crystal Structure of PCO/PE Blends.** Both thermal analysis and X-ray diffraction are used to probe the crystallization and melting behavior of the samples. Figure 3 shows the differential scanning calorimetry (DSC) heat flow (HF) thermographs during heating and wide-angle X-ray diffraction (WAXD) patterns of the PCO/PE blends with various $v^{PCO}$. It can be seen from Figure 3a that for the pure PE, there are both a major melting peak at ca. 107.0 °C and a shoulder at ca. 92.5 °C. The multiple melting peaks are normal for the pure PE probably due to the complex thermal history, which produces crystals with different perfections. With the addition of 10 vol % PCO, the shoulder disappears, while the major melting peak stays at almost the same temperature with a slightly reduced peak area. For this blend, there is also a melting peak of PCO appearing at ca. 55.5 °C. With the further increase of $v^{PCO}$, the melting peak of PE shifts to slightly lower temperatures and the peak area decreases (also shown in Figure S1, Supporting Information). At the same time, the melting peak of PCO shifts to slightly higher temperatures and the peak area increases (also shown in Figure S1, Supporting Information). For the pure PCO, the single melting peak appears at ca. 56.5 °C.

Figure 3b shows the corresponding WAXD patterns of these PCO/PE blends. It can be seen that for the pure PE, there are two strong diffraction peaks at 2$\theta$ of 21.5° and 23.7°, which are consistent with the reported values in the literature.[61−63] For the pure PCO, there are two strong diffraction peaks at 2$\theta$ of 20.2° and 23.2° and two weak peaks at 21.5° and 25.9°, which are actually consistent with the reported two strong diffraction

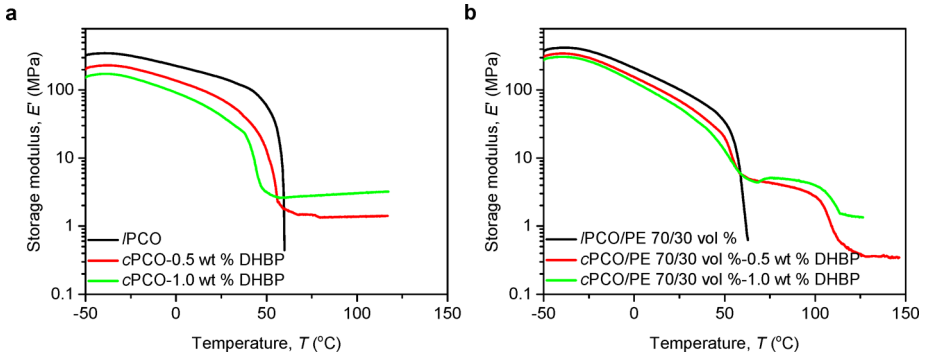


**Figure 5.** Temperature dependence of $E'$ for (a) PCO and (b) PCO/PE 70/30 vol % blends cross-linked by various $w^{DHBP}$ during heating on DMTA.

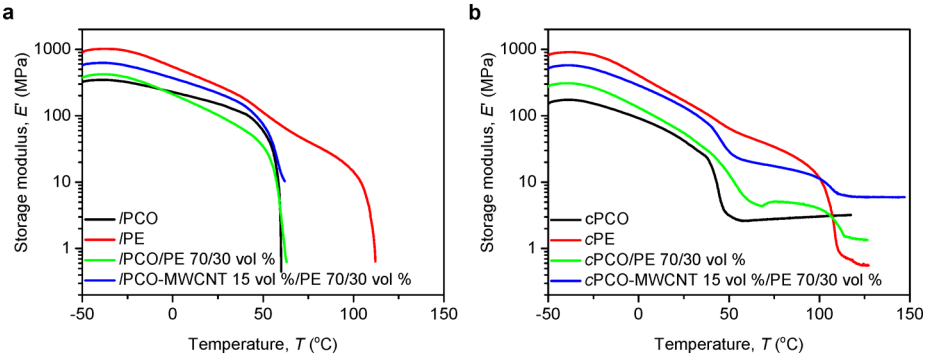


**Figure 6.** Temperature dependence of $E'$ for (a) linear and (b) cross-linked PCO, PE, PCO/PE 70/30 vol % blends, and PCO-MWCNT 15 vol %/PE 70/30 vol % nanocomposites during heating on DMTA.

peaks at 30.0° and 34.8° and two weak peaks at 31.9° and 37.0° by using different wavelength of ca. 0.2291 nm rather than ca. 0.15406 nm, which is used in this work.[53] For the blends, the diffraction peak of PCO component can be seen for the $v^{PCO}$ as low as 10 vol %, and the diffraction peak of PE component can be seen for the $v^{PCO}$ as high as 90 vol %. The change of $v^{PCO}$ causes a regular change of the diffraction peak area of the blends. However, there is no change in the $2\theta$ values of the diffraction peaks, which means that the addition of one component does not significantly change the crystal structure of the other component.

According to these results, it is clear that the miscibility between PCO and PE is quite low, and the PCO/PE blends could be taken as a typical immiscible system. This is consistent with the SEM observation, as shown in Figures 1 and 2, in which a clear boundary between the two phases can be seen.

**Control of Cross-Linking Degree by Changing the Concentration of DHBP.** The cross-linking degree of both blends and nanocomposites is controlled by changing the concentration of DHBP. Figure 4 presents the DSC HF thermographs during heating and the WAXD patterns of PCO and PCO-MWCNT 8 vol % nanocomposites and PCO/PE blends and PCO-MWCNT 15 vol %/PE 70/30 vol % nanocomposites cross-linked by various weight fraction of initiator, DHBP ($w^{DHBP}$). It can be seen from Figure 4a that the $T_m$ values of both PCO and PE in pure samples, blends, and nanocomposites decrease with increasing $w^{DHBP}$, which clearly indicates the hindrance of chemical cross-linking to the crystallization of both components (also shown in Figure S2, Supporting Information). This effect is much more significant for the PCO than for the PE: the addition of 3.0 wt % DHBP causes a $T_m$ decrease of ca. 44.0 °C for PCO but only ca. 5.0 °C for PE. Besides, the addition of 8 or 15 vol % MWCNT also decreases the $T_m$ values of both PCO and PE in all the samples, which indicates the defect effect of high contents of fillers. Figure 4b shows the corresponding WAXD patterns, and the evolution of diffraction peaks is consistent with the DSC results. By comparing the $2\theta$ values of the diffraction peaks, it can be clearly seen that the addition of MWCNT has little effect on the crystal structures of the PCO component for both pure PCO and PCO/PE blends although it does reduce the degree of crystallinity. It should be mentioned that the use of 1.0 wt % DHBP for both pure samples and blends produces an $f_g^w$ above 98 wt % which is high enough for the good SME.[64]

Figure 5 shows the temperature dependence of storage Young's modulus ($E'$) for PCO and PCO/PE 70/30 vol % blends cross-linked by various $w^{DHBP}$ during heating on dynamic mechanical thermal analyzer (DMTA). It can be clearly seen that the $E'$ below the $T_m$ decreases while that above the $T_m$ increases with increasing $w^{DHBP}$. The former is due to the decreased crystallinity, while the latter is due to the increased cross-linking degree. More detailed discussion of the thermo-mechanical properties of such samples will be given below.

**Thermo-Mechanical Properties of Pure Samples, Blends, and Nanocomposites of PCO, PE, and MWCNT.** Figure 6 shows the temperature dependence of $E'$ for linear and cross-linked PCO, PE, PCO/PE 70/30 vol % blends, and PCO-MWCNT 15 vol %/PE 70/30 vol % nanocomposites (*l*PCO, *c*PCO, *l*PE, *c*PE, *l*PCO/PE, *c*PCO/PE, *l*PCO-MWCNT/PE, and *c*PCO-MWCNT/PE, respectively) during the heating on DMTA. It can be seen that linear PCO, PE, PCO/PE blends, and PCO-MWCNT/PE nanocomposites break up at the ca. 61.0 °C, ca. 110.0 °C, ca. 63.0 °C, and ca. 62.0 °C, respectively,


dx.doi.org/10.1021/am5056307 | ACS Appl. Mater. Interfaces 2014, 6, 20051−20059

which correspond to the $T_m$ of PCO, PE, PCO, and PCO, respectively. The linear blends break up at the $T_m$ of PCO because the PCO component is the major continuous matrix and its $T_m$ is lower than that of the PE. For the cross-linked PCO and PE, there is a single step at ca. 42.0 °C and ca. 109.0 °C, respectively, which roughly correspond to the $T_m$ of PCO and PE, respectively. However, for the cross-linked PCO/PE blends, there are double steps at ca. 56.0 °C and ca. 110.0 °C, respectively. As mentioned in our previous work, the stepwise decrease of $E'$ is a typical feature of cross-linked systems.[52,65] Therefore, the double $E'$ steps indicate that both PCO and PE components in the blends are chemically cross-linked. Such samples could be used as triple SMPs with two $T_{sw}$ values of ca. 56.0 and 110.0 °C. Both the comparison between *l*PCO/PE blends and *l*PCO-MWCNT/PE nanocomposites and the comparison between *c*PCO/PE blends and *c*PCO-MWCNT/PE nanocomposites indicate that the addition of MWCNT fillers increases the $E'$ of the samples in the whole temperature range. Although the degree of crystallinity of both PCO and PE components is decreased by the addition of MWCNT fillers, the reinforcement effect of the fillers plays a more dominant role in the mechanical strength of the samples.

**Double Shape Memory Effects of Cross-Linked PCO-MWCNT Nanocomposites.** Figure 7 presents the three-dimensional (3D) diagram of three continuous shape memory cycles of cross-linked PCO-MWCNT 8 vol % nanocomposites. High reproducibility of SME can be seen by comparing the 3 cycles, especially the second and third cycles. The strain fixity ratio ($R_f$) (defined in the Supporting Information) for the three cycles is as high as ca. 98.3, 98.2, and 98.2%, respectively, and the strain recovery ratio ($R_r$, defined in the Supporting Information) for the three cycles are as high as ca. 92.2, 99.4, and 99.2%, respectively, which means the cross-linked PCO-MWCNT nanocomposites have perfect double SMEs. It should be mentioned that the $\varepsilon$ increase rather than decrease in the second step is due to the crystallization-induced elongation and might be used to get reversible SME.[54,65]

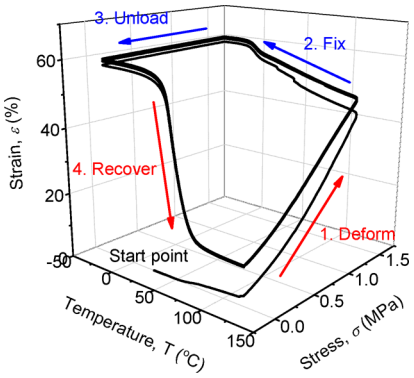


**Figure 7.** Three-dimensional (3D) diagram of three continuous shape memory cycles of cross-linked PCO-MWCNT 8 vol % nanocomposites.

**Triple Shape Memory Effects of Cross-Linked PCO/PE Blends and PCO-MWCNT/PE Nanocomposites.** Figure 8 shows the time dependence of temperature ($T$), stress ($\sigma$), and strain ($\varepsilon$) during the triple SME cycle of cross-linked PCO/PE 70/30 vol % blends and cross-linked PCO-MWCNT 15 vol %/PE 70/30 vol % nanocomposites with and without the isothermal step during heating. As shown in Figure 8a, the process is divided into 4 steps. In the first step, when $\sigma$ of 0.6 MPa is loaded at 120.0 °C, the $\varepsilon$ is increased quickly to ca. 20.6% for the blends and ca. 17.4% for the nanocomposites. During the cooling to 65.0 °C at 3.0 K min$^{-1}$ under the load, there is a small increase of $\varepsilon$ for both samples. Then, the $\sigma$ is unloaded, and the $\varepsilon$ has some decrease for both samples. In the second step, $\sigma$ is increased to 1.8 MPa at 65.0 °C, and the $\varepsilon$ is increased quickly to ca. 56.2% for the blends and ca. 28.5% for the nanocomposites. During the cooling to −30.0 °C at 3.0 K min$^{-1}$ under the load, there is a big increase of $\varepsilon$ for the blends but a small increase of $\varepsilon$ for the nanocomposites. Then, the $\sigma$ is unloaded, and the $\varepsilon$ decreases slightly for both samples. These two steps shown above are the deformation process, while the following two steps are the recovery process via heating without load. In the third step, the $\varepsilon$ decreases to ca. 23.0% for the blends and ca. 15.3% for the nanocomposites after heating to 65.0 °C. In the fourth step, the $\varepsilon$ further decreases to ca. 11.7% for the blends and ca. 8.9% for the nanocomposites after heating to 120.0 °C. The significant mechanical enhancement by adding MWCNT to the blends can be clearly seen. The $R_f(x)$, $R_f(y)$, $R_r(y \rightarrow x)$, and $R_r(x \rightarrow 0)$ for this cycle of triple SMEs are ca. 59.0, 92.7, 85.8, and 100%, respectively, for the blends. For the nanocomposites, these parameters are ca. 74.1, 93.7, 87.8, and 100%, respectively. These data indicate that both cross-linked PCO/PE blends and cross-linked PCO-MWCNT/PE nanocomposites have excellent triple SMEs and the nanocomposites are even better than the blends. Actually, these data as well as the high strain for PCO/PE system are much better than those for the PE/PP systems in our previous work mainly due to the much higher elasticity of PCO than PP.[52−56] It should be mentioned that the isothermal stay of 10 min at the end of the third step as shown in Figure 8a is used for the better recovery of the first temporary shape as widely used in the literature.[50,66,67] There is also some literature where no isothermal step is included.[68,69] Actually, such an isothermal step is not crucial to the triple SMEs of our samples, which can be clearly seen from the comparison between Figure 8a and b. For the programming without the isothermal stay, the $R_f(x)$, $R_f(y)$, $R_r(y \rightarrow x)$, and $R_r(x \rightarrow 0)$ for the blends are ca. 52.2, 95.0, 91.0, and 92.7%, respectively, while those for the nanocomposites are ca. 65.9, 91.7, 96.8, and 86.5%, respectively. Therefore, the isothermal stay is not the source of triple SMEs. The visual observation of such excellent triple SMEs will be shown below.

**Visual Observation of Triple Shape Memory Effects in Cross-Linked PCO-MWCNT/PE Nanocomposites via Both Thermal and Electrical Actuations.** Figure 9 presents the frequency dependence of electrical conductivity ($\sigma_e$) at room temperature of *l*PCO-MWCNT 8 and 15 vol %, and *c*PCO-MWCNT 15 vol % cross-linked by 0.5 and 1.0 wt % DHBP. It can be seen that all samples' $\sigma_e$ remains almost constant for the frequency of $10^2$−$10^5$ Hz, which is a typical feature of electrical conductors. Besides, the addition of MWCNT fillers causes a remarkable significant increase of $\sigma_e$ while the chemical cross-linking significantly reduces the $\sigma_e$. An increase of the fillers' volume fraction from 8 to 15 vol % causes an increase of $\sigma_e$ by ca. 4.3 times because of the formation of better conductive networks. Use of 0.5 and 1.0 wt % DHBP in the PCO-MWCNT nanocomposites causes a decrease of $\sigma_e$ by ca. 1.7 and 27.1 times, respectively, probably because of the agglomeration of fillers, formation of cracks, and even breakage of fillers, as shown in Figure 2c,d.

Visual observation is an easy way to check the triple SMEs. Figure 10 presents the photographs of cross-linked PCO-

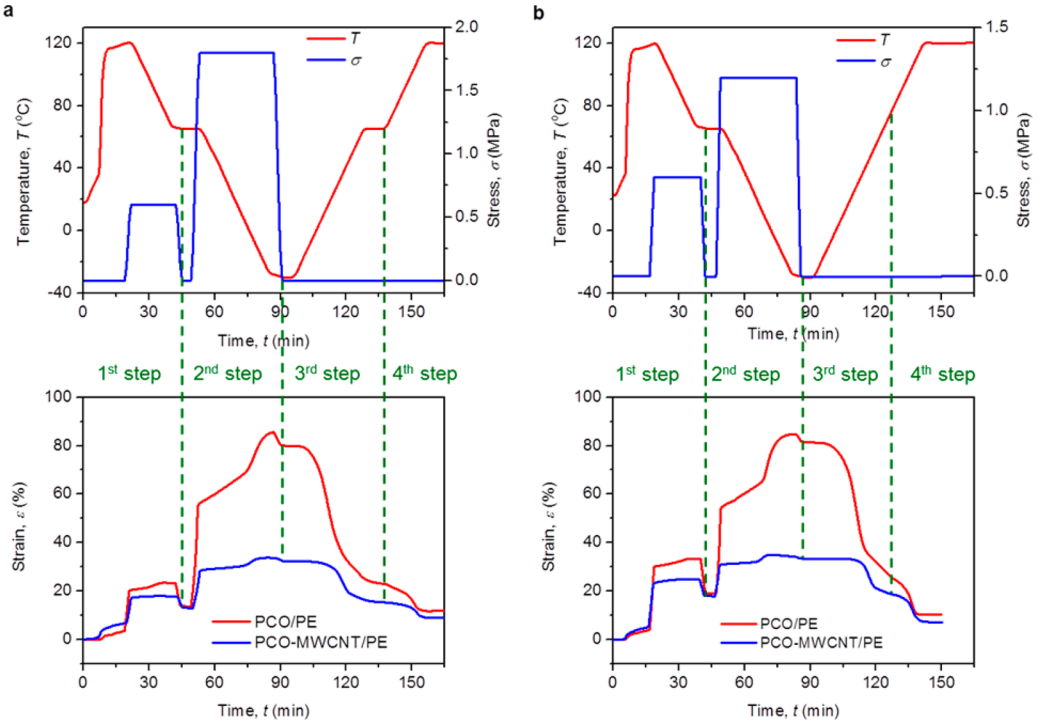


**Figure 8.** Time dependence of $T$, $\sigma$, and $\varepsilon$ during the triple SME cycle of cross-linked PCO/PE 70/30 vol % blends and cross-linked PCO-MWCNT 15 vol %/PE 70/30 vol % nanocomposites (a) with and (b) without isothermal step during the heating. The four steps are also indicated.

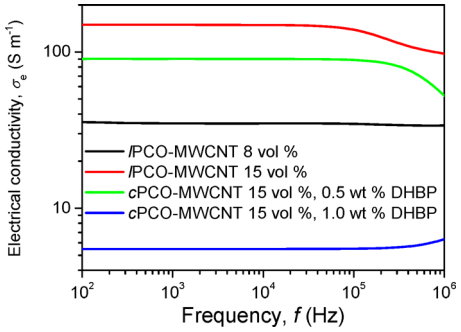


**Figure 9.** Frequency dependence of $\sigma_e$ at room temperature of *l*PCO-MWCNT 8 and 15 vol %, and *c*PCO-MWCNT 15 vol % cross-linked by 0.5 and 1.0 wt % DHBP.

MWCNT 15 vol %/PE 70/30 vol % nanocomposites in the triple SME cycle via both thermal and electrical heating. The two temporary shapes are sequentially formed at 120.0 and 60.0 °C. In the following recovery process via heating, the first temporary shape and the permanent shape are recovered in a reverse order, at 60.0 and 120.0 °C, respectively. It is clear that both the first temporary shape and the permanent shape can be almost completely recovered. Therefore, well-defined triple SMPs have been prepared in this work, and successful electrical actuation has been achieved.

As discussed in our previous work, our novel strategy of first blending two immiscible polymers to form co-continuous structure in the blends and then chemically cross-linking both components provides a simple and easy approach to realize triple SMEs.[52] Generally, appropriate separation of $T_{sw}$ is crucial to the triple SMEs. In our previous work, the $T_m$ values of the PE and PP components were ca. 110 and 165 °C, respectively.[52] In this work, PCO with a $T_m$ of ca. 55 °C is used to replace PP.[53−56] It is noteworthy that the magic number list—55, 110, and 165 with a ratio of 1/2/3—provides the same appropriate $T_m$ separation for both triple SMP systems of ca. 55 °C. In this work, not only has the purposeful control of co-continuous structure to synergically improve the system's mechanical properties been maintained, but also, the more convenient electrical actuation than thermal stimulus has been realized. Such efforts should benefit the wide industrial and medical applications of SMPs.

## CONCLUSIONS

In this work, electrically and thermally actuated triple SMPs of chemically cross-linked PCO-MWCNT/PE nanocomposites with co-continuous structure and selective distribution of fillers in PCO phase have been prepared. We have systematically studied not only the microstructure, including morphology and fillers' selective distribution in one phase of the PCO/PE blends, but also the macroscopic properties including thermal, mechanical, and electrical properties. The co-continuous window of the immiscible PCO/PE blends was found to be the $\nu^{PCO}$ of ca. 40−70 vol %. The selective distribution of fillers in one phase of co-continuous blends was obtained by a masterbatch technique and confirmed by SEM observation. The prepared triple SMP materials showed remarkable triple SMEs in the DMTA and visual observation by both thermal and electric actuations. A voltage of only 150 V was needed for the SME of PCO phase. For the strategy to prepare such polyolefin samples with well-defined microstructure, electrical actuation, and triple SMEs, the well-defined co-continuous structure in polymer blends benefited the synergetic enhancement of mechanical properties. Furthermore, the selective distribution of fillers in one phase of the blends could remarkably reduce the overall content of fillers for the same electric conductivity.


dx.doi.org/10.1021/am5056307 | ACS Appl. Mater. Interfaces 2014, 6, 20051−20059

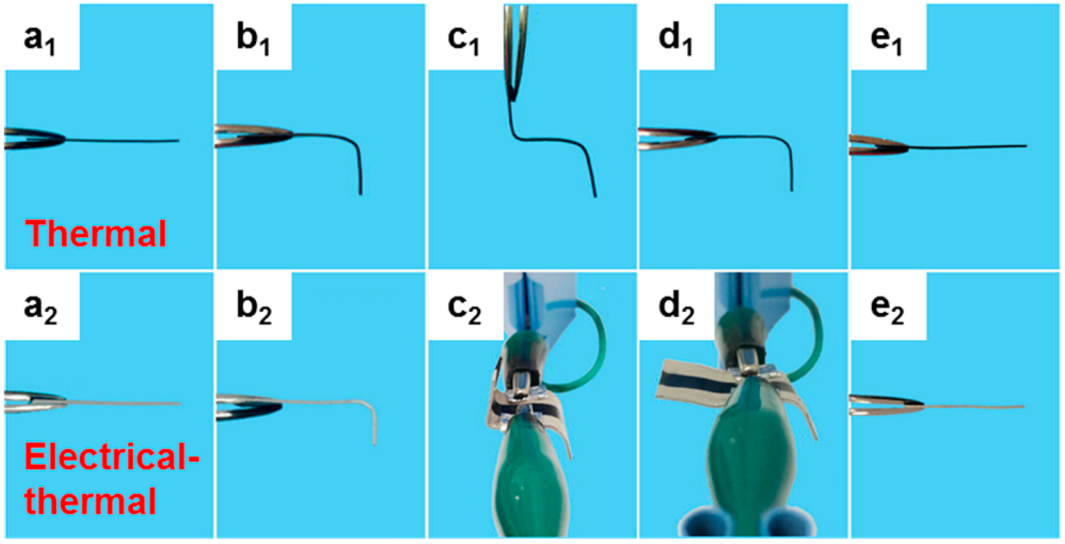


**Figure 10.** Photographs of cross-linked PCO-MWCNT 15 vol %/PE 70/30 vol % nanocomposites in the triple SME cycle of (b and c) first deformation and (d and e) following recovery: (a) permanent shape at 25.0 °C, (b) first temporary shape at 120.0 °C, (c) second temporary shape at 60.0 °C, (d) first temporary shape at 60.0 °C, (e) and permanent shape at 120.0 °C. The two opposite edges of the samples along the length in the lower row are coated with silver as electrodes. The deformation and recovery of the samples in the upper row and the deformation of the samples in the lower row was performed by thermal heating, while the recovery of the samples in the lower row was carried out by electrical heating with a voltage of 150 V for 2 min.

## ■ ASSOCIATED CONTENT

### Supporting Information

Experimental Section, dependence of $\Delta H_m$ of PCO and PE components on the $v^{PCO}$, and dependence of $T_m$ on the $w^{DHBP}$. This material is available free of charge via the Internet at http://pubs.acs.org.

## ■ AUTHOR INFORMATION

### Corresponding Authors

*Fax: +86 10 82545602. Telephone: +86 10 82545602. E-mail: zhaoj@nanoctr.cn.
*Fax: +86 10 62332599. Telephone: +86 10 62332599. E-mail: dangzm@ustb.edu.cn.
*Fax: +86 10 82618533. Telephone: +86 10 82618533. E-mail: xiadong@iccas.ac.cn.

### Present Address

[‖]National Center for Nanoscience and Technology, China, Beijing 100190, People's Republic of China.

### Notes

The authors declare no competing financial interest.

## ■ ACKNOWLEDGMENTS

This work was financially supported by the National Basic Research Program of China (973 Program, Grant No. 2014CB239500) and the Open Topic Funding of Beijing National Laboratory for Molecular Sciences. The authors acknowledge Mr. Feilong Zhang of the Institute of Chemistry, Chinese Academy of Sciences, and Ms. Xiaoyan Wang of the University of Science and Technology Beijing for their generous assistance in the measurements. The authors also acknowledge Dr. Huipeng Chen of The University of Tennessee, Knoxville, for his kind assistance with the language.

## ■ REFERENCES

(1) Hu, J.; Zhu, Y.; Huang, H.; Lu, J. Recent Advances in Shape-Memory Polymers: Structure, Mechanism, Functionality, Modeling and Applications. *Prog. Polym. Sci.* **2012**, *37*, 1720−1763.
(2) Lee, K. M.; Bunning, T. J.; White, T. J. Autonomous, Hands-Free Shape Memory in Glassy, Liquid Crystalline Polymer Networks. *Adv. Mater.* **2012**, *24*, 2839−2843.
(3) Pretsch, T.; Ecker, M.; Schildhauer, M.; Maskos, M. Switchable Information Carriers Based on Shape Memory Polymer. *J. Mater. Chem.* **2012**, *22*, 7757−7766.
(4) Li, G.; Nettles, D. Thermomechanical Characterization of a Shape Memory Polymer Based Self-Repairing Syntactic Foam. *Polymer* **2010**, *51*, 755−762.
(5) Nji, J.; Li, G. A Biomimic Shape Memory Polymer Based Self-Healing Particulate Composite. *Polymer* **2010**, *51*, 6021−6029.
(6) Sun, L.; Huang, W. M. Mechanisms of the Multi-Shape Memory Effect and Temperature Memory Effect in Shape Memory Polymers. *Soft Matter* **2010**, *6*, 4403−4406.
(7) Serrano, M. C.; Carbajal, L.; Ameer, G. A. Novel Biodegradable Shape-Memory Elastomers with Drug-Releasing Capabilities. *Adv. Mater.* **2011**, *23*, 2211−2215.
(8) Mendez, J.; Annamalai, P. K.; Eichhorn, S. J.; Rusli, R.; Rowan, S. J.; Foster, E. J.; Weder, C. Bioinspired Mechanically Adaptive Polymer Nanocomposites with Water-Activated Shape-Memory Effect. *Macromolecules* **2011**, *44*, 6827−6835.
(9) Guo, B.; Chen, Y.; Lei, Y.; Zhang, L.; Zhou, W. Y.; Rabie, A. B. M.; Zhao, J. Biobased Poly(propylene sebacate) as Shape Memory Polymer with Tunable Switching Temperature for Potential Biomedical Applications. *Biomacromolecules* **2011**, *12*, 1312−1321.
(10) Defize, T.; Riva, R.; Raquez, J.-M.; Dubois, P.; Jerome, C.; Alexandre, M. Thermoreversibly Crosslinked Poly(ε-caprolactone) as Recyclable Shape-Memory Polymer Network. *Macromol. Rapid Commun.* **2011**, *32*, 1264−1269.
(11) Ratna, D.; Karger-Kocsis, J. Shape Memory Polymer System of Semi-Interpenetrating Network Structure Composed of Crosslinked Poly(methyl methacrylate) and Poly(ethylene oxide). *Polymer* **2011**, *52*, 1063−1070.
(12) DiOrio, A. M.; Luo, X.; Lee, K. M.; Mather, P. T. A Functionally Graded Shape Memory Polymer. *Soft Matter* **2011**, *7*, 68−74.

(13) Ebara, M.; Uto, K.; Idota, N.; Hoffman, J. M.; Aoyagi, T. Shape-Memory Surface with Dynamically Tunable Nanogeometry Activated by Body Heat. *Adv. Mater.* **2012**, *24*, 273−278.
(14) Li, G.; Fei, G.; Xia, H.; Han, J.; Zhao, Y. Spatial and Temporal Control of Shape Memory Polymers and Simultaneous Drug Release Using High Intensity Focused Ultrasound. *J. Mater. Chem.* **2012**, *22*, 7692−7696.
(15) Pandini, S.; Passera, S.; Messori, M.; Paderni, K.; Toselli, M.; Gianoncelli, A.; Bontempi, E.; Ricco, T. Two-Way Reversible Shape Memory Behaviour of Crosslinked Poly(ε-caprolactone). *Polymer* **2012**, *53*, 1915−1924.
(16) Choi, J.; Ortega, A. M.; Xiao, R.; Yakacki, C. M.; Nguyen, T. D. Effect of Physical Aging on the Shape-Memory Behavior of Amorphous Networks. *Polymer* **2012**, *53*, 2453−2464.
(17) Gurevitch, I.; Silverstein, M. S. Shape Memory Polymer Foams from Emulsion Templating. *Soft Matter* **2012**, *8*, 10378−10387.
(18) Hearon, K.; Besset, C. J.; Lonnecker, A. T.; Ware, T.; Voit, W. E.; Wilson, T. S.; Wooley, K. L.; Maitland, D. J. A Structural Approach to Establishing a Platform Chemistry for the Tunable, Bulk Electron Beam Cross-Linking of Shape Memory Polymer Systems. *Macromolecules* **2013**, *46*, 8905−8916.
(19) Eisenhaure, J. D.; Xie, T.; Varghese, S.; Kim, S. Microstructured Shape Memory Polymer Surfaces with Reversible Dry Adhesion. *ACS Appl. Mater. Interfaces* **2013**, *5*, 7714−7717.
(20) Xie, T. Recent Advances in Polymer Shape Memory. *Polymer* **2011**, *52*, 4985−5000.
(21) Leng, J.; Lan, X.; Liu, Y.; Du, S. Shape-Memory Polymers and Their Composites: Stimulus Methods and Applications. *Prog. Mater. Sci.* **2011**, *56*, 1077−1135.
(22) Liu, T.; Li, J.; Pan, Y.; Zheng, Z.; Ding, X.; Peng, Y. A New Approach to Shape Memory Polymer: Design and Preparation of Poly(methyl methacrylate) Composites in the Presence of Star Poly(ethylene glycol). *Soft Matter* **2011**, *7*, 1641−1643.
(23) Meng, H.; Li, G. A Review of Stimuli-Responsive Shape Memory Polymer Composites. *Polymer* **2013**, *54*, 2199−2221.
(24) Xu, B.; Fu, Y. Q.; Ahmad, M.; Luo, J. K.; Huang, W. M.; Kraft, A.; Reuben, R.; Pei, Y. T.; Chen, Z. G.; De Hosson, J. T. M. Thermo-Mechanical Properties of Polystyrene-Based Shape Memory Nanocomposites. *J. Mater. Chem.* **2010**, *20*, 3442−3448.
(25) Zhang, Y.; Wang, Q.; Wang, C.; Wang, T. High-Strain Shape Memory Polymer Networks Crosslinked by $SiO_2$. *J. Mater. Chem.* **2011**, *21*, 9073−9078.
(26) Li, G.; Zhang, P. A Self-Healing Particulate Composite Reinforced with Strain Hardened Short Shape Memory Polymer Fibers. *Polymer* **2013**, *54*, 5075−5086.
(27) Shen, H.; Xu, Y.; Liang, F.; Gou, J.; Mabbott, B. Recovery Torque Modeling of Carbon Fiber Reinforced Shape Memory Polymer Nanocomposites. *Appl. Phys. Lett.* **2013**, *103*, 201903.
(28) Huang, W. M.; Yang, B.; Zhao, Y.; Ding, Z. Thermo-Moisture Responsive Polyurethane Shape-Memory Polymer and Composites: A Review. *J. Mater. Chem.* **2010**, *20*, 3367−3381.
(29) Du, H.; Zhang, J. Solvent Induced Shape Recovery of Shape Memory Polymer Based on Chemically Cross-Linked Poly(vinyl alcohol). *Soft Matter* **2010**, *6*, 3370−3376.
(30) He, Z.; Satarkar, N.; Xie, T.; Cheng, Y.-T.; Hilt, J. Z. Remote Controlled Multishape Polymer Nanocomposites with Selective Radiofrequency Actuations. *Adv. Mater.* **2011**, *23*, 3192−3196.
(31) Kumpfer, J. R.; Rowan, S. J. Thermo-, Photo-, and Chemo-Responsive Shape-Memory Properties from Photo-Cross-Linked Metallo-Supramolecular Polymers. *J. Am. Chem. Soc.* **2011**, *133*, 12866−12874.
(32) Lee, K. M.; Koerner, H.; Vaia, R. A.; Bunning, T. J.; White, T. J. Light-Activated Shape Memory of Glassy, Azobenzene Liquid Crystalline Polymer Networks. *Soft Matter* **2011**, *7*, 4318−4324.
(33) Yan, X.; Xu, D.; Chi, X.; Chen, J.; Dong, S.; Ding, X.; Yu, Y.; Huang, F. A Multiresponsive, Shape-Persistent, and Elastic Supramolecular Polymer Network Gel Constructed by Orthogonal Self-Assembly. *Adv. Mater.* **2012**, *24*, 362−369.
(34) Zhang, H.; Xia, H.; Zhao, Y. Optically Triggered and Spatially Controllable Shape-Memory Polymer-Gold Nanoparticle Composite Materials. *J. Mater. Chem.* **2012**, *22*, 845−849.
(35) Puig, J.; Hoppe, C. E.; Fasce, L. A.; Perez, C. J.; Pineiro-Redondo, Y.; Banobre-Lopez, M.; Lopez-Quintela, M. A.; Rivas, J.; Williams, R. J. J. Superparamagnetic Nanocomposites Based on the Dispersion of Oleic Acid-Stabilized Magnetite Nanoparticles in a Diglycidylether of Bisphenol A-Based Epoxy Matrix: Magnetic Hyperthermia and Shape Memory. *J. Phys. Chem. C* **2012**, *116*, 13421−13428.
(36) Davies, D. J. D.; Vaccaro, A. R.; Morris, S. M.; Herzer, N.; Schenning, A. P. H. J.; Bastiaansen, C. W. M. A Printable Optical Time-Temperature Integrator Based on Shape Memory in a Chiral Nematic Polymer Network. *Adv. Funct. Mater.* **2013**, *23*, 2723−2727.
(37) Zhang, H.; Zhang, J.; Tong, X.; Ma, D.; Zhao, Y. Light Polarization-Controlled Shape-Memory Polymer/Gold Nanorod Composite. *Macromol. Rapid Commun.* **2013**, *34*, 1575−1579.
(38) Jung, Y. C.; Yoo, H. J.; Kim, Y. A.; Cho, J. W.; Endo, M. Electroactive Shape Memory Performance of Polyurethane Composite Having Homogeneously Dispersed and Covalently Crosslinked Carbon Nanotube. *Carbon* **2010**, *48*, 1598−1603.
(39) Xiao, Y.; Zhou, S.; Wang, L.; Gong, T. Electro-Active Shape Memory Properties of Poly(ε-caprolactone)/Functionalized Multi-walled Carbon Nanotube Nanocomposite. *ACS Appl. Mater. Interfaces* **2010**, *2*, 3506−3514.
(40) Luo, X.; Mather, P. T. Conductive Shape Memory Nanocomposites for High Speed Electrical Actuation. *Soft Matter* **2010**, *6*, 2146−2149.
(41) Yu, Z.; Zhang, Q.; Li, L.; Chen, Q.; Niu, X.; Liu, J.; Pei, Q. Highly Flexible Silver Nanowire Electrodes for Shape-Memory Polymer Light-Emitting Diodes. *Adv. Mater.* **2011**, *23*, 664−668.
(42) Le, H. H.; Schoss, M.; Ilisch, S.; Gohs, U.; Heinrich, G.; Pham, T.; Radusch, H.-J. CB Filled EOC/EPDM Blends as a Shape-Memory Material: Manufacturing, Morphology, and Properties. *Polymer* **2011**, *52*, 5858−5866.
(43) Fei, G.; Li, G.; Wu, L.; Xia, H. A Spatially and Temporally Controlled Shape Memory Process for Electrically Conductive Polymer−Carbon Nanotube Composites. *Soft Matter* **2012**, *8*, 5123−5126.
(44) Luo, X.; Mather, P. T. Triple-Shape Polymeric Composites (TSPCs). *Adv. Funct. Mater.* **2010**, *20*, 2649−2656.
(45) Bae, C. Y.; Park, J. H.; Kim, E. Y.; Kang, Y. S.; Kim, B. K. Organic−Inorganic Nanocomposite Bilayers with Triple Shape Memory Effect. *J. Mater. Chem.* **2011**, *21*, 11288−11295.
(46) Radusch, H.-J.; Kolesov, I.; Gohs, U.; Heinrich, G. Multiple Shape-Memory Behavior of Polyethylene/Polycyclooctene Blends Cross-Linked by Electron Irradiation. *Macromol. Mater. Eng.* **2012**, *297*, 1225−1234.
(47) Bai, Y.; Jiang, C.; Wang, Q.; Wang, T. Multi-Shape-Memory Property Study of Novel Poly(ε-Caprolactone)/Ethyl Cellulose Polymer Networks. *Macromol. Chem. Phys.* **2013**, *214*, 2465−2472.
(48) Chatani, S.; Wang, C.; Podgorski, M.; Bowman, C. N. Triple Shape Memory Materials Incorporating Two Distinct Polymer Networks Formed by Selective Thiol-Michael Addition Reactions. *Macromolecules* **2014**, *47*, 4949−4954.
(49) Xie, T. Tunable Polymer Multi-Shape Memory Effect. *Nature* **2010**, *464*, 267−270.
(50) Li, J.; Xie, T. Significant Impact of Thermo-Mechanical Conditions on Polymer Triple-Shape Memory Effect. *Macromolecules* **2011**, *44*, 175−180.
(51) Ware, T.; Hearon, K.; Lonnecker, A.; Wooley, K. L.; Maitland, D. J.; Voit, W. Triple-Shape Memory Polymers Based on Self-Complementary Hydrogen Bonding. *Macromolecules* **2012**, *45*, 1062−1069.
(52) Zhao, J.; Chen, M.; Wang, X.; Zhao, X.; Wang, Z.; Dang, Z.-M.; Ma, L.; Hu, G.-H.; Chen, F. Triple Shape Memory Effects of Cross-Linked Polyethylene/Polypropylene Blends with Cocontinuous Architecture. *ACS Appl. Mater. Interfaces* **2013**, *5*, 5550−5556.

(53) Liu, C.; Chun, S. B.; Mather, P. T.; Zheng, L.; Haley, E. H.; Coughlin, E. B. Chemically Cross-Linked Polycyclooctene: Synthesis, Characterization, and Shape Memory Behavior. *Macromolecules* **2002**, *35*, 9868−9874.
(54) Chung, T.; Romo-Uribe, A.; Mather, P. T. Two-Way Reversible Shape Memory in a Semicrystalline Network. *Macromolecules* **2008**, *41*, 184−192.
(55) Kunzelman, J.; Chung, T.; Mather, P. T.; Weder, C. Shape Memory Polymers with Built-in Threshold Temperature Sensors. *J. Mater. Chem.* **2008**, *18*, 1082−1086.
(56) Thakur, V. K.; Vennerberg, D.; Kessler, M. R. Green Aqueous Surface Modification of Polypropylene for Novel Polymer Nanocomposites. *ACS Appl. Mater. Interfaces* **2014**, *6*, 9349−9356.
(57) Le, H. H.; Osswald, K.; Ilisch, S.; Hoang, X. T.; Heinrich, G.; Radusch, H.-J. Master Curve of Filler Localization in Rubber Blends at an Equilibrium State. *J. Mater. Sci.* **2012**, *47*, 4270−4281.
(58) Cao, J.-P.; Zhao, X.; Zhao, J.; Zha, J.-W.; Hu, G.-H.; Dang, Z.-M. Improved Thermal Conductivity and Flame Retardancy in Polystyrene/Poly(vinylidene fluoride) Blends by Controlling Selective Localization and Surface Modification of SiC Nanoparticles. *ACS Appl. Mater. Interfaces* **2013**, *5*, 6915−6924.
(59) Zhao, X.; Zhao, J.; Cao, J.-P.; Wang, X.; Chen, M.; Dang, Z.-M. Tuning the Dielectric Properties of Polystyrene/Poly(vinylidene fluoride) Blends by Selectively Localizing Carbon Black Nanoparticles. *J. Phys. Chem. B* **2013**, *117*, 2505−2515.
(60) Cao, J.-P.; Zhao, J.; Zhao, X.; You, F.; Yu, H.; Hu, G.-H.; Dang, Z.-M. High Thermal Conductivity and High Electrical Resistivity of Poly(vinylidene fluoride)/Polystyrene Blends by Controlling the Localization of Hybrid Fillers. *Compos. Sci. Technol.* **2013**, *89*, 142−148.
(61) Nojima, S.; Kiji, T.; Ohguma, Y. Characteristic Melting Behavior of Double Crystalline Poly(ε-caprolactone)-*block*-polyethylene Copolymers. *Macromolecules* **2007**, *40*, 7566−7572.
(62) Inci, B.; Lieberwirth, I.; Steffen, W.; Mezger, M.; Graf, R.; Landfester, K.; Wagener, K. B. Decreasing the Alkyl Branch Frequency in Precision Polyethylene: Effect of Alkyl Branch Size on Nanoscale Morphology. *Macromolecules* **2012**, *45*, 3367−3376.
(63) Pepels, M. P. F.; Hansen, M. R.; Goossens, H.; Duchateau, R. From Polyethylene to Polyester: Influence of Ester Groups on the Physical Properties. *Macromolecules* **2013**, *46*, 7668−7677.
(64) Ortega, A. M.; Yakacki, C. M.; Dixon, S. A.; Likos, R.; Greenberg, A. R.; Gallcd, K. Effect of Crosslinking and Long-Term Storage on the Shape-Memory Behavior of (Meth)acrylate-Based Shape-Memory Polymers. *Soft Matter* **2012**, *8*, 7381−7392.
(65) Wang, X.; Zhao, J.; Chen, M.; Ma, L.; Zhao, X.; Dang, Z.-M.; Wang, Z. Improved Self-Healing of Polyethylene/Carbon Black Nanocomposites by Their Shape Memory Effect. *J. Phys. Chem. B* **2013**, *117*, 1467−1474.
(66) Chen, S.; Yuan, H.; Ge, Z.; Chen, S.; Zhuo, H.; Liu, J. Insights into Liquid-Crystalline Shape-Memory Polyurethane Composites Based on an Amorphous Reversible Phase and Hexadecyloxybenzoic Acid. *J. Mater. Chem. C* **2014**, *2*, 1041−1049.
(67) Bai, Y.; Zhang, X.; Wang, Q.; Wang, T. A Tough Shape Memory Polymer with Triple-Shape Memory and Two-Way Shape Memory Properties. *J. Mater. Chem. A* **2014**, *2*, 4771−4778.
(68) Bellin, I.; Kelch, S.; Langer, R.; Lendlein, A. Polymeric Triple-Shape Materials. *Proc. Natl. Acad. Sci. U.S.A.* **2006**, *103*, 18043−18047.
(69) Torbati, A. H.; Nejad, H. B.; Ponce, M.; Sutton, J. P.; Mather, P. T. Properties of Triple Shape Memory Composites Prepared via Polymerization-Induced Phase Separation. *Soft Matter* **2014**, *10*, 3112−3121.